Geolocation Algorithm for Earth Observation Sensors Onboard the International Space Station

Changyong Dou, Xiaodong Zhang, Hojin Kim, Jaganathan Ranganathan, Doug Olsen, and Huadong Guo

Abstract

As a near orbit space platform, the International Space Station (ISS) has been increasingly used for Earth observing applications. This paper presents a quaternion-based forward geolocation algorithm for Earth observing sensors onboard the ISS. The input parameters include the orbital state and attitude information of the ISS and the look vector of the sensor. The proposed algorithm agrees with the commercial navigation product, Satellite Tool Kit®, within 0.5 m in ideal situations. The inherent uncertainties in ISS attitude and state determinations, and the International Space Station Agriculture Camera (ISSAC) tilting angle were estimated to introduce an error less than 800 m. However, the actual geolocation error evaluated using the images obtained by the ISSAC is roughly 4 km, much greater than the inherent uncertainty and mainly due to (a) delay caused by the Windows® operating system in acquiring images, and (b) the misalignment of the ISSAC sensor coordinate system with the ISS body-fixed coordinate system. A preliminary cal/val process using the Google Earth™ as reference was performed to quantify these two errors, the correction of which improved the geolocation accuracy to 500 m, well within the inherent uncertainty.

Introduction

International Space Station (ISS) manifests an international collaboration involving the efforts of 16 countries to maintain a long term human presence in outer space. The ISS provides a platform for scientific experiments in a wide range of disciplines including life and biology sciences, physics and materials science, space products and developments, and human and environment interaction (Jules, 2008). The ISS can also serve as an Earth observation platform. For example, the Crew Earth Observations (CEO) mission allows the photographs taken by the crewmembers to be publicly accessible, supporting a variety of studies including urban growth (Robinson *et al.*, 2000) and vegetation dynamics (Stefanov *et al.*, 2003). However, the difficulties in geo-referencing these images restrict their usage for wider remote sensing applications (Robinson *et al.*, 2002).

Compared to a satellite, the ISS offers some unique characteristics for Earth observing applications: a relatively low Earth orbit varying between 350 and 420 km potentially delivering a higher spatial resolution, an orbital inclination of 51.6 degrees covering approximately 75 percent of the inhabited land surface of the Earth, and an orbital period of 90 minutes allowing passes over the same location in approximately every three days (Gebelein and Eppler, 2006). Additionally, unlike sensors onboard a satellite, the payload on the ISS can be serviced and repaired (if necessary) through space shuttle flights.

Taking advantage of the ISS as an Earth observing platform, many sensor systems have been designed and deployed. For example, FOCUS is an infrared sensor of European Space Agency (ESA) that is dedicated to monitoring high temperature events of volcanic activity, pollutant gas emissions, and forest fires (Tank *et al.*, 2001). The Earth Viewing Camera (EVC), located in the European Technology Exposure Facility, captures color images of the Earth surface both in daylight and at nighttime with a ground sampling distance (GSD) of 100 m (Reibaldi *et al.*, 2004). The Station High-sensitivity Ocean Research Experiment (SHORE) is a multi-band optical spectrometer, acquiring images with a GSD of approximately 15 m over coral reefs, atolls, tidal areas, and shore/ocean interfaces (Jacobson, 2007). The Hyperspectral Imager for the Coastal Ocean (HICO) system, sponsored by the Office of Naval Research, is a visible and shortwave infrared hyperspectral sensor for monitoring coastal zone environment (such as water clarity, bathymetry, or coral reefs), the maritime atmosphere, and distribution of fires and active volcanoes (Corson *et al.*, 2010).

The International Space Station Agriculture Camera (ISSAC) is a multi-spectral digital imaging system specifically designed for the use onboard the ISS. Sponsored by the National Aeronautics and Space Administration's (NASA) Education Office, ISSAC was designed and developed by students at the University of North Dakota primarily for precision farming and natural resource management. The ISSAC

Changyong Dou is with the Institute of Remote Sensing and Digital Earth, Chinese Academy of Sciences, No. 9 Dengzhuang South Road, Haidian, Beijing 100094, PR China, and the University of Chinese Academy of Sciences, Beijing, PR China (cydou@coede.ac.cn; hdguo@ceode.ac.cn).

Xiaodong Zhang is with the Department of Earth System Science and Policy, University of North Dakota, Grand Forks, ND 58202.

Hojin Kim, Jaganathan Ranganathan, and Doug Olsen are with the Northern Great Plains Center for People and Environment, University of North Dakota, Grand Forks, ND 58202.

Huadong Guo is with the Institute of Remote Sensing and Digital Earth, Chinese Academy of Sciences, No. 9 Dengzhuang South Road, Haidian, Beijing 100094, PR China.

Photogrammetric Engineering & Remote Sensing
Vol. 79, No. 7, July 2013, pp. 625–637.

0099-1112/13/7907–625/$3.00/0

was built using commercial-off-the-shelf (COTS) products taking images at three spectral bands of green, red, and near-infrared matching the Landsat-5 TM sensor's bands 2, 3, and 4 but with a higher GSD of about 15 m (versus the 30 m of Landsat). The imaging system was launched using the Japanese H-II Transfer Vehicle (HTV-2) to the ISS in January 2011.

To fully utilize the potential offered by these Earth observing sensors, the imagery needs to be georeferenced. The objective of this study was to develop, and evaluate its performance, i.e., a geolocation algorithm for images acquired by an Earth observing sensor onboard the ISS. While the algorithm was originally developed for the ISSAC, it can be easily modified to suit the need of other ISS payloads as well.

Algorithm Overview

An forward geolocation algorithm for a remote sensing application typically starts with the orbital state (position and velocity) and attitude information (roll, pitch, and yaw angles) of the platform, which, combined with sensor position and orientation information, are used to calculate the geographic location on Earth where the sensor is looking at through a series of transformation of coordinate systems (CSs), including sensor, spacecraft body-fixed, spacecraft orbital, Earth Centered Inertial (ECI), and Earth Centered Rotating (ECR). Transforming from the spacecraft body-fixed CS to the spacecraft orbital CS requires the spacecraft attitude information (Jacobson, 2007; Wolfe *et al.*, 2002). For the transformation from the spacecraft orbital to the ECI, either one of two sets of information can be used: the orbital state defined in the ECI CS (Wolfe *et al.*, 2002), or the inclination, longitude of the ascending node, the perigee, and the true anomaly (Jacobson, 2007). In transforming from ECI to ECR, again, either one of two sets of information can be used: the ephemeris (polar motion, sidereal time, astronomic nutation, and precession) (Wolfe *et al.*, 2002), or the Greenwich Mean Sidereal time (Jacobson, 2007).

The geolocation algorithm proposed in this paper uses orbital state and attitude of the ISS, the ISSAC look vector, and the Earth terrain surface (an ideal Earth reference ellipsoid overlaid with a Digital Elevation Model (DEM)) to compute the geographic coordinates in latitude, longitude, and altitude. The key of the algorithms is to transform the sensor look vector, by the method of unit quaternion, from the Sensor CS to the ECR CS from which the geographic position is determined as the intersection of the transformed sensor look vector with the Earth terrain surface. The common steps (Wolfe *et al.*, 2002) would use the location and velocity vectors in ECI CS and ephemeris information to transform from the orbital to ECI CSs and from ECI to ECR CSs, respectively. Since the ISS also provides its location and velocity vectors in ECR CS, our algorithm took advantage of this piece of information by transforming the ISS orbital CS to the ECR CS directly, bypassing the intermediate steps of orbital to ECI and ECI to ECR transformation and thus avoiding the use of the Earth rotation and the ISS ephemeris information, i.e., polar motion, sidereal time, astronomic nutation, and precession.

Quaternion

A quaternion, $q = (r, xi, yj, zk)$, denotes a vector in a four-dimensional space defined by one real axis and three orthogonal complex axes of i, j, k, obeying Hamilton's rules. Or alternatively, $q = (r, v)$, with $q = (0, v)$ defining a pure quaternion. The conjugate of $\boldsymbol{q}$, $q^* = (r, -xi, -yj, -zk)$ or $q^* = (r, -v)$ (Hart *et al.*, 1994).

There are different methods for specifying vector rotations and coordinate system orientations, such as orthonormal matrices, axis/angle, Euler angles, and quaternion. We choose quaternion mainly because it has an advantage among others of avoiding potential gimbal lock during CS transformation (Hanson, 2000). Another reason is that the ISS Broadcast Ancillary Data (BAD) packages provide the ISS's attitude parameters in quaternion format.

It is mathematically easy to perform an arbitrary rotation about an arbitrary axis using quaternion without gimbal lock issue because the rotation is performed in 4D space. The rotation of a vector $\bar{V}_{in}$ in 3D (or as a pure quaternion of $(0, \bar{V}_{in})$ in 4D) about an arbitrary axis, $[x, y, z]$, to $\bar{V}_{out}$ by an angle θ can be performed by (Hanson, 2000):

$$(0, \bar{V}_{out}) = q\,(0, \bar{V}_{in})q^*, \tag{1}$$

where $\boldsymbol{q}$ and its conjugate $\boldsymbol{q}^*$, are defined as:

$$\begin{aligned} q &= \cos(\theta/2) + (xi + yj + zk).\sin(\theta/2)/\sqrt{x^2 + y^2 + z^2} \\ q^* &= \cos(\theta/2) - (xi + yj + zk).\sin(\theta/2)/\sqrt{x^2 + y^2 + z^2} \end{aligned} \tag{2}$$

respectively. Note that $\boldsymbol{q}$ and $\boldsymbol{q}^*$ are also unit quaternion by definition.

International Space Station

As the largest man-made object in the outer space, the ISS rely on two independent systems, one by the United States and the other by Russia, for its Guidance, Navigation, and Control (GN&C). One of the main functions of US GN&C system is to determine the state and attitude of the ISS. The ISS's orbital state is monitored by two Space Integrated Global Positioning System Inertial Navigation System (SIGI) receiver/processors (an array of four antennas), and a constellation of 26 Global Positioning Systems (GPS). The GPS interferometry technique, combined with two rate gyro assemblies, is used to determine the ISS attitude and its rate of changing (Polites and Bartlow, 1997).

Compared to a conventional satellite, the ISS experiences a much greater change in its attitude due to its lower orbit. Sometimes, the attitude is adjusted on purpose to meet specific operational requirements. For example, dockings and un-dockings of space shuttles from different countries will need special attitudes (Vajdos *et al.*, 2004). Typically defined in an ECI CS (e.g., J2000) for satellites, the orbital state data for the ISS is also directly defined in the ECR CS. The ISS orbital state and the attitude, along with others critical orbital information, are available to onboard ISS users through the BAD by the GN&C flight software and recorded on the ground at the Houston Mission Control Center, which can be accessed through the Orbiter Data Reduction Complex (ODRC) database. For geolocation, the required parameters from GN&C are the instantaneous orbital state and attitude information of the ISS at the time of image acquisition.

ISSAC System

The ISSAC is situated in the Window Observational Research Facility (WORF) within the US Laboratory Module, and has a build-in mechanism of tilting up to ±30° in the general cross-track direction, allowing repeated visit of a target within a day. The ISSAC sensor has been radiometrically and spectrally calibrated (Olsen *et al.*, 2010) and imagery is available to public free of charge through the Digital Northern Great Plains (Zhang *et al.*, 2010).

The ISSAC imaging device consists of a Sigma Macro lens (f/2.8, Sigma Corporation of America, Ronkonkoma, New York) with a focal length of 150 mm, a three-way glass prism splitting the incident light into three spectral bands (Green: 515 – 600 nm; Red 630 – 700 nm; Near Infrared: 740 – 910 nm), and three CCD arrays, each of 1,392 × 1,040 (cross-track × along-track) pixels and each pixel at a size of

6.45 microns (Olsen *et al.*, 2011). After the assembly of the system, the focal length was determined to be 133.25 mm, about 11 percent shorter than the manufacturer's value. This configuration gives a field of view angle of 2.88° and 3.85° in along- and cross-track directions, respectively (Figure 1). At a nominal ISS altitude of 350 km, an ISSAC image covers an area of 15.65 km × 20.95 km. For geolocation, the required parameters regarding the ISSAC include the acquisition time, the pixel location in the CCD array plane and its off-nadir tilting angle.

Coordinate System

Five coordinate systems (CS) (Sauceda *et al.*, 2001) are involved in the proposed geolocation algorithm.

Sensor (or Camera) CS

The Sensor CS (Figure1) has its origin located at the lens, with the optical axis as Z axis, Z_{AC}, positively pointing to nadir direction of ISS, X_{AC} parallel to the X axis of ISS body-fixed CS, and Y_{AC} completed by the right hand rule. Ideally, the Sensor CS should be in the exact alignment with the ISS body-fixed CS, with the exception of shift in the origin. The origin of Sensor CS is also called the projection center of the camera.

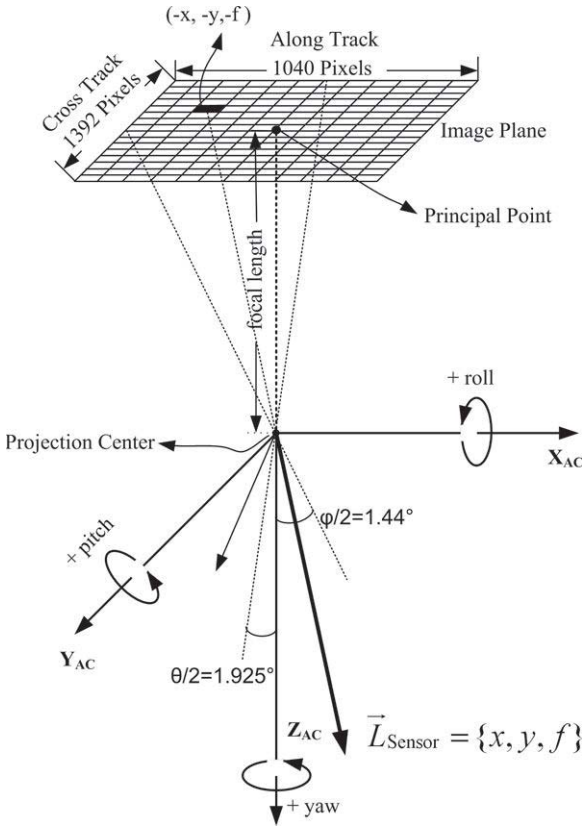

Figure 1. The Sensor Coordinate System and a look vector of sensor defined in it. The origin of the Sensor CS is the projection center at the optical axis, the Z axis (Z_{AC}) is along the optical axis positively pointing to nadir direction of ISS, the X axis (X_{AC}) is parallel to the X axis of ISS body-fixed CS, and Y axis (Y_{AC}) is completed by right hand rule. Ideally, the Sensor CS should align with ISS body-fixed CS, with a shift in the origin determined by the ISSAC offset position in the ISS body-fixed CS.

ISS Body-fixed CS

The ISS body-fixed CS (Figure 2) is a right-handed Cartesian system, with its origin located at the ISS center of mass, with X_{ISS} axis pointing to the general forward direction in parallel to the longitudinal axis of the module cluster, and Y_{ISS} axis pointing to the starboard direction in parallel to the Integrated Truss Segment (ITS) S0. The Z_{ISS} axis completes the right-handed Cartesian system in the direction of nadir.

Local Vertical and Local Horizontal CS

The Local Vertical and Local Horizontal (LVLH) CS (Figure 3) is referenced to the ISS's orbit plane, where the ISS is represented as a mass point. The origin of LVLH is located at the ISS center of mass. The X_{LVLH}-Z_{LVLH} plane is the instantaneous orbit plane at the time of interest, with Z_{LVLH} pointing toward the center of the Earth. The Y_{LVLH} axis is normal to the orbit plane. The X_{LVLH} axis completes the right-handed orthogonal system, positive in the direction of the ISS motion.

The ISS body-fixed CS, whose axes rotate with the ISS attitude, can be derived from the Local Vertical and Local Horizontal CS, and their relationship is defined by the Euler angles in the sequence of yaw, pitch, and roll around Z_{ISS}, Y_{ISS}, and X_{ISS} axis, respectively.

Conventional Terrestrial Reference System CS

Conventional Terrestrial Reference System (CTRS) CS (Figure 4) is an ECR CS co-rotating with the Earth in its diurnal motion in space. This Earth-fixed coordinate system also has been corrected for polar motion and variable Earth rotation to account for the true rotation and wobble of the Earth's spin axis about a mean axis. The CTRS removes or corrects for any known surface deformation or velocities including solid Earth tides, ocean tide loading, plate tectonics, and for some of stations, atmospheric loading effects. The Z_{CTRS} axis is coincident with the Earth's principal rotation axis and positive toward the Conventional International Origin (CIO). The positive X_{CTRS} axis passes through the intersection of the CTRS reference equatorial plane and the CTRS reference meridian. The positive Y_{CTRS} axis completes the right-handed Cartesian system.

Geodetic Coordinate System

Geodetic Coordinate System (Figure 5) is an ECR CS based on an Earth reference ellipsoid. Strictly speaking, it is not a coordinate system, because no origin is specified. But, it is assumed its origin coincide with the origin of CTRS.

The WGS84 is an ideal Earth reference ellipsoid which does not account for any topography. The DEM is a digital representation of the Earth's surface created from terrain elevation data. The combination of WGS84 and the DEM will be referred as the Earth reference ellipsoid.

Coordinate System Transformation and Geographic Location Determination

The forward geolocation algorithm transforms the sensor look vector, defined under the Sensor CS, into CTRS CS, from which geographic coordinates can be determined. In addition to the sensor look vector, the attitude and the position and velocity vectors for the ISS at a given moment are needed and can be extracted from the BAD packages broadcasted every second in the ISS.

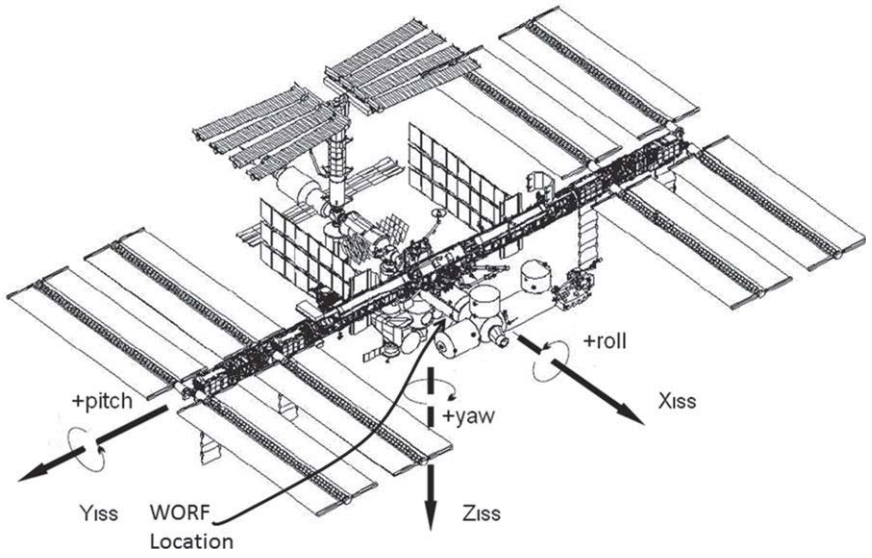

Figure 2. ISS Body-fixed Coordinate System. With the rotation Euler angles sequence of yaw, pitch, and roll around Z_{ISS}, Y_{ISS}, and X_{ISS}, respectively, the ISS Body-fixed CS can be derived from the LVLH CS. The WORF is located in the US module within ISS.

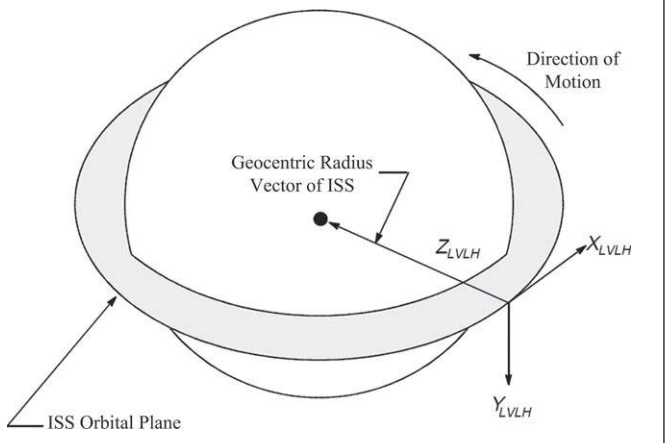

Figure 3. Local Vertical and Local Horizontal (LVLH) Coordinate System. The ISS can be considered as a mass point, and X_{LVLH}-Z_{LVLH} plane is the instantaneous orbit plane. Z_{LVLH} axis lies along the geocentric radius vector to the ISS and is positive toward to the center of the Earth. The Y_{LVLH} axis is normal to the orbit plane. The X_{LVLH} axis completes the right-handed orthogonal system and the positive in the direction of the ISS motion.

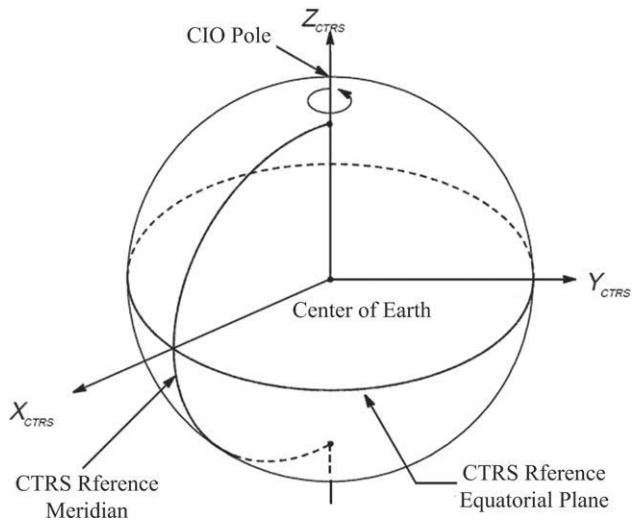

Figure 4. Conventional Terrestrial Reference System (CTRS) Coordinate System. The Z_{CTRS} axis is coincident with the Earth's principal rotation axis and the positive direction is directed toward the Conventional International Origin (CIO). The positive X_{CTRS} axis passes through the intersection of the CTRS reference equatorial plane and the CTRS reference meridian. The positive Y_{CTRS} axis completes the rotating right-handed Cartesian system.

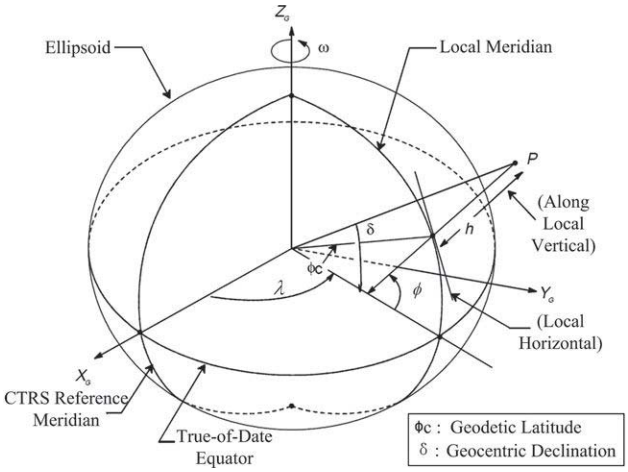

Figure 5. Geodetic Coordinate System. For a point of interest *P*, a line, known as the Geodetic Local Vertical, is defined as perpendicular to the ellipsoid from point *P*. *h*, geodetic altitude, is the distance from point *P* to the reference ellipsoid, measured along the geodetic local vertical, and is positive for points outside the ellipsoid. λ is longitude measured in the plane of the Earth's true equator from the prime (Greenwich) meridian to the local meridian, measured positive eastward. ϕd is the geodetic latitude, measured in the plane of the local meridian from the Earth's true equator to the geodetic local vertical, measured positive north from the equator.

ISSAC Look Vector Defined in the Sensor CS

As shown in Figure 1, a look vector is defined as an imaginary line starting from an arbitrary ISSAC CCD pixel, whose coordinate is (*–x, –y, –f*), passing through the projection center (i.e., the origin of the sensor CS). The look vector is denoted as $\vec{L}_{Sensor} = \{x, y, f\}$ (Lee *et al.*, 2000). The ranges for *x* and *y* are [–520 × 6.45, 520 × 6.45] (μm) and [–696 × 6.45, 696 × 6.45] (μm), respectively, (where the value of 6.45 μm is the size of one CCD pixel, 520 one-half of the number of CCD pixels in *X* direction and 696 one-half of the number in *Y* direction), and *f* is the focal length (= 133.25 mm). The ISSAC has an ability of tilting in cross-track direction, or in other words, the vector $\vec{L}_{Sensor}$ rotates about the X_{AC} axis. The tilted look vector $\vec{L}_{Sensor\ Tilt}$ can be found:

$$(0, \vec{L}_{Sensor\ Tilt}) = q_{Tilt}(0, \vec{L}_{Sensor})\ q_{Tilt}^{*} \tag{3}$$

where $q_{Tilt} = (\cos(\psi/2), \sin(\psi/2), 0, 0)$, and $q_{Tilt}^{*} = (\cos(\psi/2), -\sin(\psi/2), 0, 0)$, with ψ denoting the tilting angle (cross-track).

If the ISSAC (or other payload system) had the tilting ability in along-track direction, the $\vec{L}_{Sensor\ Tilt}$ would be rotated about Y_{AC} axis.

Transformation from Sensor to ISS Body-fixed CS

If we assume that the ISSAC system was installed in such a way that the coordinates of the Sensor and ISS body-fixed CSs are aligned with each other in the same directions, then the transformation from Sensor CS to ISS body-fixed CS is just a shift in the origin. But, in reality, there is always misalignment between the two coordinate systems. Assuming that by rotating the Sensor CS by the angles of roll (*r*), pitch (*p*), and yaw (*y*) angles around its *X, Y,* and *Z* axes, the two CSs will be aligned with each other, the corresponding unit quaternion for this rotation, $\boldsymbol{q}_{Sensor} = (r_0, xi, yj, zk)$, can be defined as (Hanson, 2000):

$$\begin{aligned} r_0 &= \cos(r/2)\cos(p/2)\cos(y/2) - \sin(r/2)\sin(p/2)\sin(y/2) \\ x &= \sin(r/2)\cos(p/2)\cos(y/2) + \cos(r/2)\sin(p/2)\sin(y/2) \\ y &= \cos(r/2)\sin(p/2)\cos(y/2) - \sin(r/2)\cos(p/2)\sin(y/2) \\ z &= \cos(r/2)\cos(p/2)\sin(y/2) + \sin(r/2)\sin(p/2)\cos(y/2) \end{aligned} \tag{4}$$

Let $\vec{V}_{Sensor}$ denote an arbitrary vector defined in the Sensor CS and $\vec{V}_{ISS}$ is its corresponding vector in the ISS body-fixed CS, to find $\vec{V}_{ISS}$ we follow:

$$(0, \vec{V}_{ISS}) = q_{Sensor}^{*}\ (0, \vec{V}_{Sensor}) q_{Sensor}. \tag{5}$$

Without losing generality, $\vec{V}_{Sensor}$ can represent the look vector of the ISSAC defined in Sensor CS or a look vector for the other payload. Let $\vec{S}_{ISS} = \{X_0, Y_0, Z_0\}$ denote the position of ISSAC (or any payload), where X_0, Y_0, and Z_0 are the ISSAC offset values in the ISS body-fixed CS. The transformation from Sensor to ISS body-fixed CS can be performed as:

$$(0, \vec{V}_{ISS}) = q_{Sensor}^{*}\ (0, \vec{V}_{Sensor}) q_{Sensor} + (0, \vec{S}_{ISS}) \tag{6}$$

Transformation from ISS Body-fixed to LVLH CS

The instantaneous state of the ISS Body-fixed CS might deviate from LVLH, with deviation defined by three rotation angles, i.e., yaw, pitch, and roll, around the, *Z, Y,* and *X* axes of the ISS body-fixed CS, respectively (Figure 2). Similar to Equations 4 and 5, to transform a vector ($\vec{V}_{ISS}$) defined in the ISS body-fixed CS to that ($\vec{V}_{LVLH}$) in LVLH, we follow:

$$\begin{aligned} &(0, \vec{V}_{ISS}) = q_{ISS}\ (0, \vec{V}_{LVLH})\ q_{ISS}^{*} \\ &\Rightarrow \qquad . \\ &(0, \vec{V}_{LVLH}) = q_{ISS}^{*}\ (0, \vec{V}_{ISS})\ q_{ISS} \end{aligned} \tag{7}$$

The transformation quaternion is broadcasted through the ISS BAD packages. But the broadcasted quaternion, $\boldsymbol{q}_{LVLH}$, is defined as from LVLH to ISS body-fixed CS, i.e., $q_{LVLH} = q_{ISS}^{*}$. Therefore, to apply it:

$$(0, \vec{V}_{LVLH}) = q_{LVLH}\ (0, \vec{V}_{ISS})\ q_{LVLH}^{*}. \tag{8}$$

Transformation from LVLH to CTRS CS

The relationship between LVLH and CTRS can be defined by two vectors describing the position ($\vec{p}_{CTRS}$) and the velocity ($\vec{v}_{CTRS}$) of the ISS in CTRS (Figure 6-1):

$$\begin{aligned} Z_{LVLH} &= -\vec{p}_{CTRS} \\ Y_{LVLH} &= Z_{LVLH} \times \vec{v}_{CTRS}\ . \\ X_{LVLH} &= Y_{LVLH} \times Z_{LVLH} \end{aligned} \tag{9}$$

The transformation from LVLH to CTRS involves several rotations illustrated in Figure 6. The first rotation is to rotate LVLH about Z_{LVLH} such that X_{LVLH} is in the plane defined by X_{CTRS} and Z_{LVLH}. The rotation angle γ (Figure 6-1) can be found as:

$$\gamma = \arccos(Y_{LVLH} \cdot X_{CTRS} \times \vec{p}_{CTRS}). \tag{10}$$

If X_{CTRS} and Z_{LVLH} are parallel or anti-parallel, then γ will be zero. The values of γ determined above range from 0 to π; but since rotation through quaternion always follows the right-hand rule, the actual rotation angles range from 0 to 2π. The general rule is: if $(\vec{V}_{begin} \times \vec{V}_{end}) \cdot \vec{R}_{axis} \geq 0$ then the rotation angle falls in $0 - \pi$, else the angle falls in $\pi - 2\pi$, where $\vec{V}_{begin}$

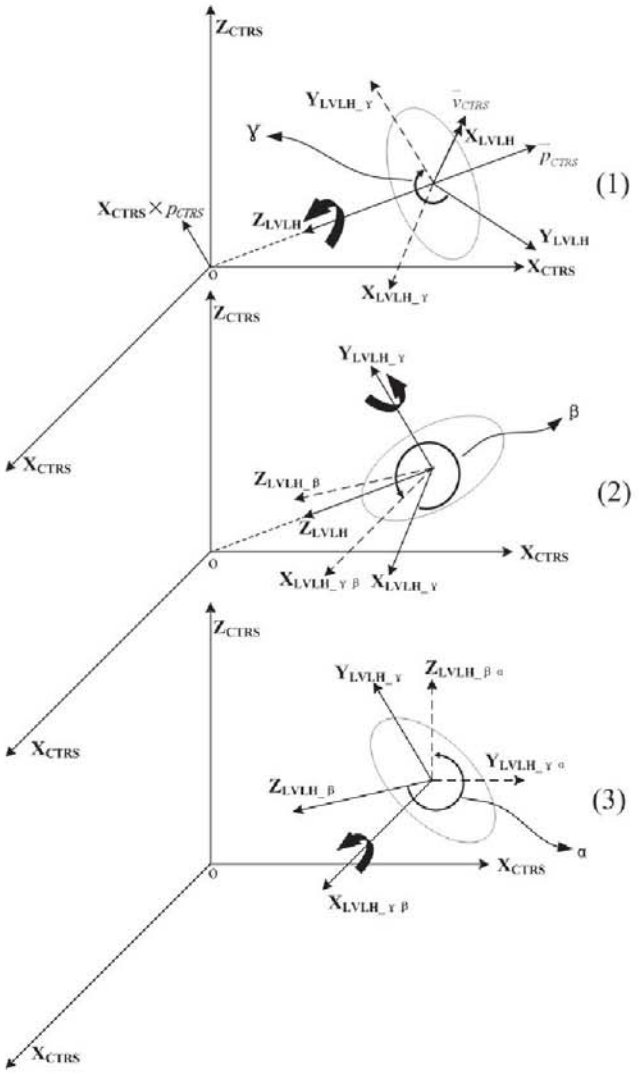

Figure 6. Steps of the transformation from LVLH to CTRS Coordinate System. The LVLH coordinate system is defined by the position and velocity vectors of the ISS in CTRS. The first rotation is to rotate LVLH about ZLVLH with angle γ such that X_{LVLH} is the same plane defined by XCTRS and ZLVLH (1). The second rotation is to rotate LVLH about Y_{LVLH_r} with angle β to align X_{LVLH_r} with X_{CTRS} (2). The third rotation is to rotate the LVLH about X_{LVLH_rB} with angle α to align Z_{LVLH_B} with Z_{CTRS} (3). At the completion of three rotations, the three axes of the new LVLH coordinate system X_{LVLH_rB}, Y_{LVLH_rA}, and Z_{LVLH_BA}, align with the respective axes of CTRS. The last step is to shift the origin of LVLH to that of CTRS, which is not shown in this figure.

denotes the vector to be rotated about the axis $\vec{R}_{axis}$ to $\vec{V}_{end}$. Therefore, the quaternion for this rotation is:

$$q_\gamma = \cos(\gamma/2) + (p_X i + p_Y j + p_Z k)\sin(\gamma/2)/\sqrt{p_X{}^2 + p_Y{}^2 + p_Z{}^2} \quad (11)$$

where p_x, p_y, and p_z are the components of $\vec{p}_{CTRS}$. Following Equation 1, the rotations of X_{LVLH} and Y_{LVLH} can be performed:

$$\begin{aligned}(0, X_{LVLH\_\gamma}) &= q_\gamma (0, X_{LVLH}) q_\gamma^* \\ (0, Y_{LVLH\_\gamma}) &= q_\gamma (0, Y_{LVLH}) q_\gamma^*\end{aligned} \quad (12)$$

where X_{LVLH_γ} and Y_{LVLH_γ} are the new axes after rotation.

The second rotation is to rotate the LVLH about Y_{LVLH_γ} to align X_{LVLH_γ} with X_{CTRS} (Figure 6-2). The rotation angle β can be found:

$$\beta = \arccos(X_{LVLH\_\gamma} \cdot X_{CTRS}). \quad (13)$$

The quaternion of the rotation is:

$$q_\beta = \cos(\beta/2) + (Y_{-\gamma x} i + Y_{-\gamma y} j + Y_{-\gamma z} k)\sin(\beta/2)/\sqrt{Y_{-\gamma x}{}^2 + Y_{-\gamma y}{}^2 + Y_{-\gamma z}{}^2} \quad (14)$$

where $Y_{-\gamma x}$, $Y_{-\gamma y}$, and $Y_{-\gamma z}$ is the component of the Y_{LVLH_γ} axis. Rotating Z_{LVLH} and X_{LVLH_γ} following:

$$\begin{aligned}(0, X_{LVLH\_\gamma\beta}) &= q_\beta (0, X_{LVLH\_\gamma}) q_\beta^* \\ (0, Z_{LVLH\_\beta}) &= q_\beta (0, Z_{LVLH}) q_\beta^*\end{aligned} \quad (15)$$

where $X_{LVLH\_\gamma\beta}$ and Z_{LVLH_β} are the new axes after rotation.

The third rotation is to rotate the LVLH about X_{LVLH_γ} to align Z_{LVLH_β} with Z_{CTRS} (Figure 6-3). The rotation angle is $\alpha = \arccos(Z_{LVLH\_\beta} \cdot Z_{CTRS})$. The quaternion of the rotation, q_α, is

$$q_\alpha = \cos(\alpha/2) + (X_{-\gamma\beta x} i + X_{-\gamma\beta y} j + X_{-\gamma\beta z} k)\sin(\alpha/2)/\sqrt{X_{-\gamma\beta x}{}^2 + X_{-\gamma\beta y}{}^2 + X_{-\gamma\beta z}{}^2} \quad (16)$$

where $X_{-\gamma\beta x}$, $X_{-\gamma\beta y}$, and $X_{-\gamma\beta z}$ is the component of $X_{LVLH\_\gamma\beta}$ axis. Rotating Z_{LVLH_β} and Y_{LVLH_γ} according to:

$$\begin{aligned}(0, Y_{LVLH\_\gamma\alpha}) &= q_\alpha (0, Y_{LVLH\_\gamma}) q_\alpha^* \\ (0, Z_{LVLH\_\beta\alpha}) &= q_\alpha (0, Z_{LVLH\_\beta}) q_\alpha^*.\end{aligned} \quad (17)$$

At the completion of three rotations, the three axes of the new LVLH CS, $X_{LVLH\_\gamma\beta}$, $Y_{LVLH\_\gamma\alpha}$, and $Z_{LVLH\_\beta\alpha}$, align with the respective axes of CTRS. The last step is to shift the origin of LVLH to that of CTRS. It follows that for a vector $\vec{V}_{LVLH}$ in the LVLH coordinate system, the corresponding vector representation $\vec{V}_{CTRS}$ in the CTRS coordinate system can be derived as:

$$(0, \vec{V}_{CTRS}) = q_\gamma^* q_\beta^* q_\alpha^* (0, \vec{V}_{LVLH}) q_\alpha q_\beta q_\gamma + (0, \vec{p}_{CTRS}). \quad (18)$$

Geolocation Calculation

The geographic location on Earth is defined by the intersection of the sensor look vector and the Earth reference ellipsoidal surface, which, in this study, is a combination of WGS84 ellipsoid and a DEM. There are three steps involved: (1) transformation of the sensor look vector, initially defined in the Sensor CS, to the CTRS CS, (2) calculation of the intersection of the look vector with the ideal Earth reference ellipsoid, denoted as geodetic location, and (3) calculation of "true" geographic location by searching for the intersection between the look vector and the DEM. The separation of Steps 2 and 3 is necessary because a DEM is always defined relative to the underlying Earth reference ellipsoid (or geoid).

Transformation of Sensor Look Vector

To transform $\vec{L}_{Sensor}$ and $\vec{S}_{ISS}$ defined in the Sensor and ISS body-fixed CSs into $\vec{L}_{CTRS}$ and $\vec{S}_{CTRS}$ in the CTRS CS, we combine Equations 3, 6, 8, and 18:

$$\begin{aligned}(0, \vec{S}_{CTRS}) &= q_\gamma^* q_\beta^* q_\alpha^* q_{LVLH} (0, \vec{S}_{ISS}) q_{LVLH}{}^* q_\alpha q_\beta q_\gamma + (0, \vec{p}_{CTRS}) \\ (0, \vec{L}_{CTRS}) &= q_\gamma^* q_\beta^* q_\alpha^* q_{LVLH} (q_{Sensor}{}^* q_{Tilt}) (0, \vec{L}_{Sensor}) q_{Tilt}{}^* q_{Sensor} \\ &\quad + (0, \vec{S}_{ISS})) q_{LVLH}{}^* q_\alpha q_\beta q_\gamma + (0, \vec{p}_{CTRS}).\end{aligned} \quad (19)$$

The line L(x, y, z) defined by sensor look vector can be formed as:

$$\begin{bmatrix} x \\ y \\ z \end{bmatrix} = \vec{S}_{CTRS} + t \cdot \vec{D}_{CTRS} \tag{20}$$

where $\vec{D}_{CTRS} = \vec{L}_{CTRS} - \vec{S}_{CTRS}$ and t is a parametric number. $\vec{D}_{CTRS}$ denotes the direction of the line passing through the point $\vec{S}_{CTRS}$ and in parallel with $\vec{L}_{CTRS}$, whose intersection with the Earth surface model determines the geodetic location on Earth.

Geodetic Location with the Ideal Earth Reference Ellipsoid

The WGS84 Earth reference ellipsoid E(x, y, z) is defined as:

$$\begin{bmatrix} x^2 \\ y^2 \\ z^2 \end{bmatrix} \begin{bmatrix} \frac{1}{a^2} \\ \frac{1}{b^2} \\ \frac{1}{c^2} \end{bmatrix} = 1 \tag{21}$$

where a and b ($a = b$) are the semi-major (equator) radius of the Earth, and c is the semi-minor (polar) radius of the WGS84 Earth reference ellipsoid.

In general, there are two intersections between the line L(x, y, z) and the Earth reference ellipsoid E(x, y, z). The solution with the smaller distance to the ISS is the geodetic location. Given the determined intersection (x_{geo}, y_{geo}, z_{geo}), its geographic location, i.e., latitude (ϕ) and longitude (λ), is calculated as (Rosborough *et al.*, 1994):

$$\begin{aligned} \phi &= \arctan\left(\frac{z_n}{\rho - w}\right) \\ \lambda &= \arctan 2(y_{geo}/x_{geo}) \end{aligned} \tag{22}$$

where $\rho = \sqrt{x_{geo}^2 + y_{geo}^2} / a$ and $z_n = z/a$, and w is determined through an iterative process until the estimates of w_{new} and w_{old} converge,

$$w_{new} = e^2(\rho - w_{old}) / \sqrt{(\rho - w_{old})^2 + (1 - e^2)z_n^2}. \tag{23}$$

It is typically assumed the first guess of w_{old} to be 0. In Equation 23, $e = \sqrt{1 - c^2/a^2}$ is the eccentricity of the Earth reference ellipsoid (WGS84).

With the geographic latitude (ϕ), the Earth surface elevation can be determined by the following equation:

$$h = \frac{L}{\sin\phi} - R_N \tag{24}$$

where $R_N = a / \sqrt{1 - e^2 \sin^2\phi}$, and $L = z + e^2 R_N \sin\phi$.

Geographic Location with the Real Earth Terrain Surface

The latitude (ϕ) and longitude (λ) determined above is the intersection between sensor look vector and an ideal Earth reference ellipsoid; at this particular point, the elevation, h (Equation 24), is zero. To calculate the geographic location, a DEM has to be used. We will use an iterative method, summarized in Figure 7, to find the intersection of the look vector and the terrain surface.

Let (x_{geo}, y_{geo}, z_{geo}), determined in the previous section, denote the first guess of the geographic location (φ_0, λ_0, h_0 (= 0)). We then find the next location (x, y, z) along the viewing direction by slightly extending the length of the initial location vector (x_{geo}, y_{geo}, z_{geo}), from which we find a new geographic location (φ_1, λ_1, h_1) by applying Equations 22, 23, and 24. The corresponding DEM elevation at (φ_1, λ_1) is h_1'. Typically h_1 is less than h_1' because the initial locations are still "inside"

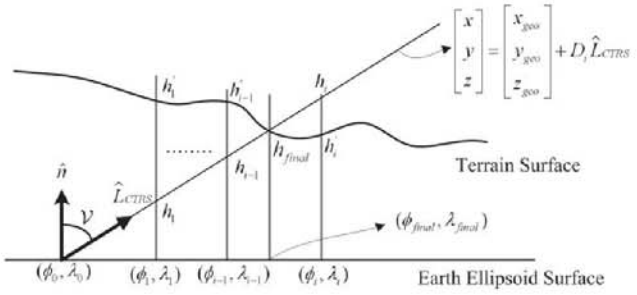

Figure 7. The illustration of the iteration in finding the geographic location. The first guess is the geographic location (ϕ_0, λ_0, h_0 (= 0)). The second guess is moved along $\hat{L}_{CTRS}$ to a new location with a small step length. The latitude, longitude, and elevation (ϕ_1, λ_1, h_1) of the new location are calculated, and the corresponding DEM elevation (h_1') at (ϕ_1, λ_1) is compared with h_1. This process is repeated until $|h_i| > |h_i'|$. The final geographic location (ϕ_{final}, λ_{final}, h_{final}) can be determined by the last two iterations.

the terrain. The process is repeated until $|h_i| > |h_i'|$. The reason of using absolute values for comparison is to accommodate the cases where the terrain is below the reference with negative values in elevation. Mathematically, the new location (x, y, z) at the i^{th} iteration is calculated as:

$$\begin{bmatrix} x \\ y \\ z \end{bmatrix} = \begin{bmatrix} x_{geo} \\ y_{geo} \\ z_{geo} \end{bmatrix} + D_i \hat{L}_{CTRS} \tag{25}$$

where $\hat{L}_{CTRS} = -\frac{\vec{L}_{CTRS}}{|\vec{L}_{CTRS}|}$, and D_i represents the incremental extension of the vector length. Also, $D_i = D_{i-1} + ds/\sin V$ ($D_0 = 0$), ds represents a step length on the ideal Earth reference ellipsoid surface, and v is the angle between the local ellipsoid normal unit vector $\hat{n}$ ($\hat{n} = (\cos\phi\cos\lambda, \cos\phi\sin\lambda, \sin\phi)$) and $\hat{L}_{CTRS}$. Once the iteration stops, the intersection between the look vector and the terrain can be computed from the last two iterations (N–1 and N):

$$\begin{aligned} h_{final} &= kh_N + (1\text{–}k)h_{N-1} = kh'_N + (1\text{–}k)h'_{N-1} \\ D_{final} &= D_N - kds \\ \begin{bmatrix} x \\ y \\ z \end{bmatrix}_{final} &= \begin{bmatrix} x_{geo} \\ y_{geo} \\ z_{geo} \end{bmatrix} + D_{final} \hat{L}_{CTRS} \end{aligned} \tag{26}$$

Results and Discussion

The operation of ISSAC is controlled through the Science Operation Center (SOC) at the University of North Dakota. A preliminary evaluation of our geolocation algorithm is shown in Plate 1, where the ISS ground tracks are plotted along with ISSAC nadir pixel footprints calculated with the tilting angle (ψ in Equation 3) set to be –30°, 0°, and 30°, respectively, and assuming that the Sensor and the ISS body-fixed CSs are perfectly aligned with each other (i.e., set r, p, and y in Equation 4 to zero) with zeros offset (i.e., set $\vec{S}_{ISS}$ in Equation 6

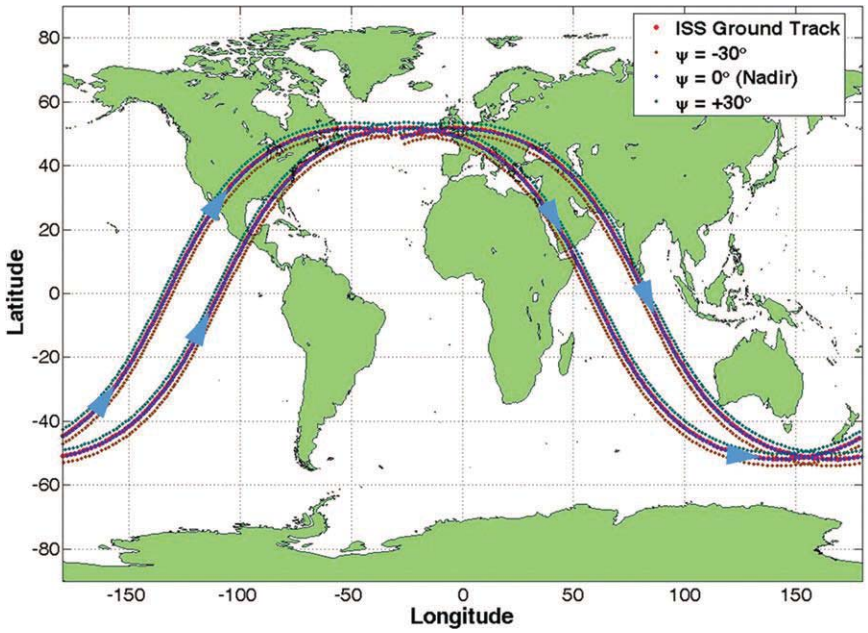

Plate 1. The ISS and ISSAC ground tracks. The ISS ground tracks are plotted along with ISSAC nadir pixel locations calculated with the pointing angle set to be −30°, 0° and 30°, respectively, and the offset position set to be zero. The input parameters, including location and velocity vectors of ISS in CTRS and the ISS attitude quaternion, were extracted from the ISS BAD packages for a time period from 2008:320:00:00:00 (yyyy:ddd:hh:mm:ss) to 2008:320:03:10:00 at an interval of every 20 seconds.

to zero). The input parameters, including location and velocity vectors and attitude quaternion of ISS, were extracted from the ISS BAD packages for a time period from 2008:320:00:00:00 (yyyy:ddd:hh:mm:ss) to 2008:320:03:10:00 at an interval of 20 seconds. As can be expected and clearly shown, the ISSAC nadir footprint roughly overlaps with the ISS ground track, and the ISSAC tracks of −30° and 30° tilting angles lie along the ISS flight direction in the right and left sides respectively.

Tables 1 and 2 summarize a more comprehensive evaluation of the performance of the geolocation algorithm. Table 1 lists the relevant orbital information of four ISS positions that are randomly chosen from an ISS orbit using the commercial Satellite Tool Kit® (STK; Analytical Graphics, Inc.). For each ISS position, four ISSAC nadir point location are tested, i.e., $\psi = 0°$, 10°, −20°, and 30°. For each combination of the ISS position and the ISSAC view, the pixel location on Earth surface is calculated using the STK and our algorithm; and Table 2 summarizes their comparison. The differences in both longitude and latitude between our algorithm and the commercial STK are less than ~0.5 m for all the cases tested. These results (Table 2) demonstrate the accuracy that can be achieved by the geolocation algorithm under ideal situations. In reality, there are many factors that can potentially affect its accuracy, such as terrain topography, the uncertainties in the ISS parameters and the systematic biases caused by the ISSAC system.

Plate 2 shows two images acquired by the ISSAC, over Kennedy Space Center, Florida (Plate 2a) and Stanton, North Dakota (Plate 2c) at 13:06:28:52 (hh:mm:ss:ms) on 05 August (local time) and at 18:06:20:57 on 09 September 2011 with off-nadir tilting angle of −24.729° and 21.163°, respectively. The ground sampling distances of the two images are 24.13 m × 21.59 m (cross-track×along-track) and 27.38 m × 18.53 m, respectively. The images were geolocated using our algorithm with DEM from the Shuttle Radar Topographic Mission (SRTM) data, and the results are overlaid onto the Google Earth™. In calculation, we have assumed that the Sensor CS coincides with the ISS body-fixed CS because we do not know the

Table 1. The Input Parameters of ISS's Position, Velocity, and Attitude used in Computing the Geographic Locations shown in Table 2

Case	Time(GMT)	Position (km)			Velocity(m/s)			Attitude (degree)		
	yyyy:ddd:hh:mm:ss	X	Y	Z	X	Y	Z	Pitch	Roll	Yaw
1	2011:001:00:10:00	−6582.85088	−1264.77025	−626.202207	272.36	−4332.347	5995.967	−2.60972	1.07869	−3.85759
2	2011:001:00:30:00	−1357.72013	−4268.74667	5009.780001	7161.517	−78.342	1867.401	−2.6945	1.31885	−4.09209
3	2011:001:00:42:00	3706.105595	−3212.31277	4595.652.924	6155.307	2863.764	−2951.964	−2.66238	1.15043	−4.19301
4	2011:001:00:58:00	6708.363684	510.588544	−213.259676	−505.48	4260.585	−6034.295	−2.45742	0.758885	−4.17757

Table 2. The Nadir Point Geographic Locations Estimated by STK and our Algorithm for the Four Set of Input Parameters listed in Table 1, each with Four Tilting Angles (Ψ) of the ISSAC Sensor. Longitude and Latitude are in Degrees, but their Differences are in Meters

Case	Time (GMT) yyyy:ddd:hh:mm:ss	Looking Angle/degree	0 (Nadir) Lat	0 (Nadir) Lon	10 Lat	10 Lon	−20 Lat	−20 Lon	30 Lat	30 Lon
1	2011:001:00:10:00	STK	−5.465237	−169.252172	−5.166195	−169.73464	−6.077083	−168.263123	−4.468714	−170.857985
		Our Alg.	−5.465239	−169.252176	−5.166195	−169.734644	−6.077085	−168.263127	−4.468713	−170.85799
		Difference(m)	0.22	0.44	0	0.44	0.22	0.44	−0.11	0.44
2	2011:001:00:30:00	STK	48.388742	−107.894412	48.894119	−108.278581	47.353962	−107.135316	50.071768	−109.210751
		Our Alg.	48.388741	−107.894413	48.894118	−108.27858	47.353962	−107.135317	50.071767	−109.21075
		Difference(m)	0.02	0.11	0.02	−0.11	0	0.11	0.01	−0.11
3	2011:001:00:42:00	STK	43.457451	−41.05251	43.950968	−40.675368	42.445967	41.805131	45.099779	−39.770402
		Our Alg.	43.45745	−41.052509	43.950967	−40.675367	42.445966	41.80513	45.09979	−39.7704
		Difference(m)	0.03	−0.11	0.03	−0.11	0.04	−0.11	0.03	−0.22
4	2011:001:00:58:00	STK	−1.659201	4.298238	−1.334926	4.731384	−2.434346	3.40742	−0.497184	5.736313
		Our Alg.	−1.695201	4.298237	−1.334925	4.731384	−2.434346	3.40742	−0.497184	5.736313
		Difference(m)	0	0.11	−0.11	0	0	0	0	0

exact offset and orientation (or misalignment) of the ISSAC Sensor CS with respect to the ISS body-fixed CS. Apparently, the geolocated images do not match exactly with the target. The disagreement between the geolocated ISSAC images and Google Earth™ can be summarized into three categories: (a) a displacement in along-track direction, (b) a displacement in cross-track direction, and (c) a rotational displacement of entire image. Table 3 summarized the errors in each category. It is noted that the rotational displacement varies with the orbital orientation: clockwise for descending case (Plate 2a) and counter-clockwise for the ascending case (Plate 2c).

The possible sources of error in geolocation include the uncertainties in determination of the ISS ephemeral parameters, off-nadir tilting angle, image acquisition time, and ISSAC offset position and orientation in the ISS body-fixed CS. While the first three factors are random in nature, the last one is systematic once the ISSAC is installed. The ISS ephemeral parameters needed by the geolocation algorithm include the ISS attitude in the quaternion format in the LVLH CS, and the position and velocity vectors of ISS, both defined in the CTRS CS. The US GN&C system could determine the attitude of ISS with an accurate of 0.25° per axis, and a recent SIGI firmware update improved the accuracy to 0.1° per axis. The fourth release of GN&C software ensures the accuracies of position and velocity vectors are 6 m per axis and 20 m/s, respectively. The time accuracy after the SIGI firmware update is within 20 to 50 microseconds. Assuming a 6 m per axis uncertainty in the determination of ISS position, the induced error in geolocation would be about 5 m. The geolocation error due to a 20 m/s uncertainty in the determination of ISS velocity would be about 30 m. The uncertainty of 0.1° in the attitude determination would translate into an error of about 700 m. The ISSAC can tilt in the cross-track directions at an angle up to ±30° with an uncertainty of one hundredth of a degree which translates to a ground location error of about 70 m in the cross-track direction. Combining together all these potential error sources that are due to the uncertainty in determination of the ISS ephemeral parameters and the ISSAC tilting angle, the geolocation error is on the order of 800 m, which accounts for only a fraction of the actual errors shown in Plate 2a and 2c and Table 3. So far, we have assumed that the ISSAC Sensor CS is in perfect alignment with the ISS body-fixed CS. In reality, it is impossible to ensure or enforce this conformation. While translational offset in the origins of the two CSs can introduce an error of up to 10 m, the rotational offset in the axes would cause a significant geolocational error on the ground. Therefore, we concluded that the observed geolocation error exhibited in Plate 2a and 2c is largely due to the remaining uncertainties in registration of image acquisition time and the rotational offset of ISSAC within the ISS.

Quantifying the remaining uncertainties typically requires a comprehensive cal/val (calibration/validation) process (Wolfe *et al.*, 2002; Wiebe *et al.*, 2002; Poe *et al.*, 2008; Kieffer *et al.*, 2008). Since the ISSAC project, sponsored by NASA Education Office, is mainly for education/training purpose, it is beyond our means to conduct such a campaign, which would entail tremendous effort to collect the Ground Control Points (GCPs) and to analyze the data. On the other hand, the existing errors in the geolocation results need to be corrected, or at least understood, for the algorithm to be useful.

A preliminary cal/val experiment using Google Earth™ as a reference, whose accuracy is about 20 m in US (Potere, 2008), was conducted to evaluate the two remaining uncertainties: the temporal offset in image acquisition, and the rotational offset in the orientation of the ISSAC with respect to the ISS body fixed CS. In addition, the latter is defined by three angles: the misalignments between the ISSAC Sensor and ISS body-fixed CS in the X-axis (roll), in the Y-axis (pitch), and in the Z-axis (yaw) (see Figure 1). The Microsoft Windows® environment in which the image acquisition software ran is not a real-time operating system. Therefore, there is always a temporal offset between the issuing of a command and the actual execution of the command. The net effect of this uncertainty on geolocation is to cause an along-track shift (category 1), which, unfortunately, could also be caused by the ISSAC pitch angle misalignment, even though the former is expected to be random while the latter more or less systematic. Since it is difficult for us to separate these two, we simply assumed that the along-track offset was due entirely to the temporal uncertainty in image acquisition, which also implies an assumption

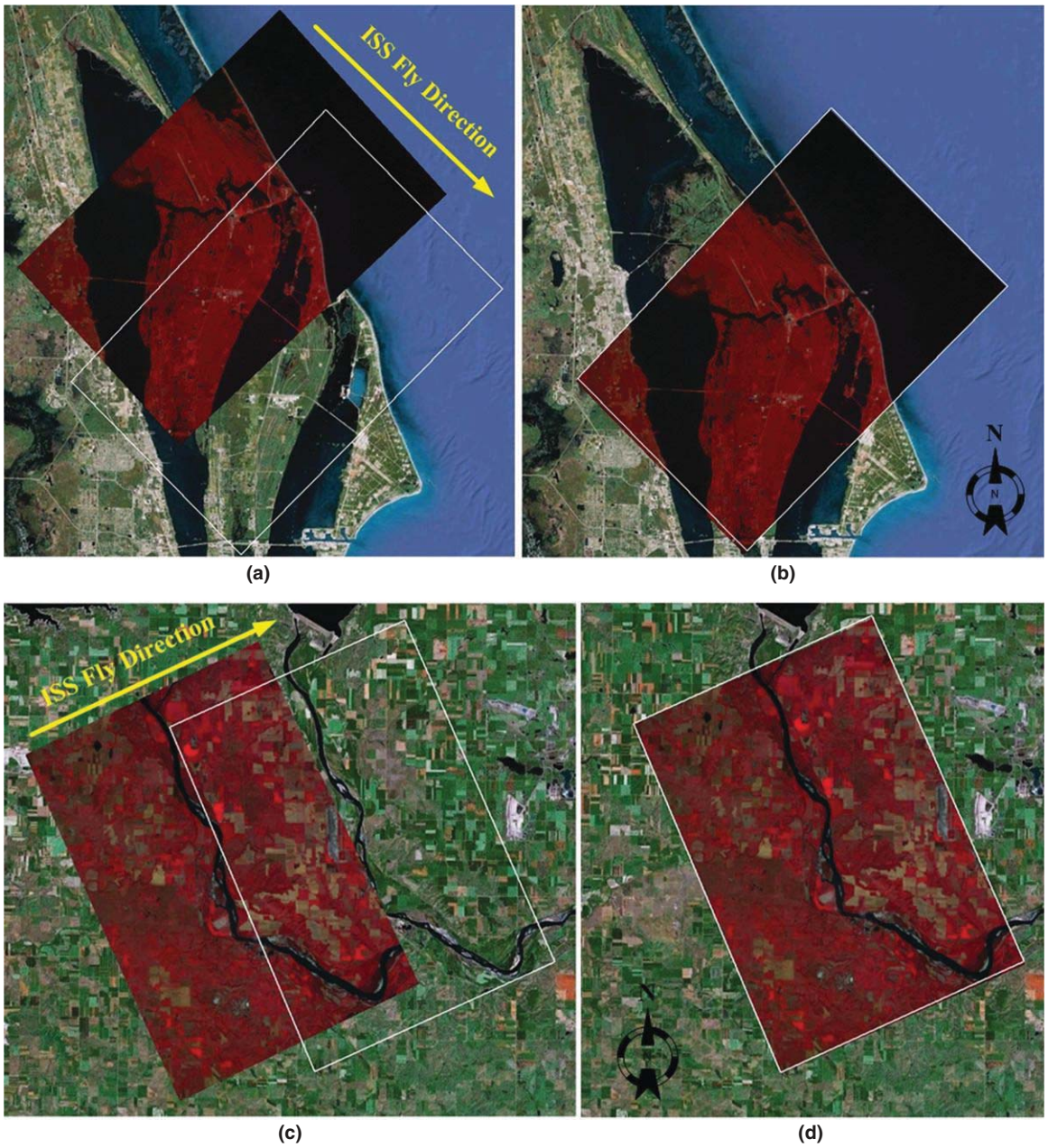

Plate 2. Two ISSAC images acquired over Kennedy Space Center, Florida at 13:06:28:52 (hh:mm:ss:ms) on 05 August 2011 (local time) with a sensor tilting angle of –24.729°: (a) over Stanton, North Dakota, at 18:06:20:57 on 09 September 2011 with a tilting angle of 21.163, and (b) The geolocated images are overlaid onto the Google Earth™. The white squares denote the coverage of the images, if they were to be shifted to match the Google Earth™.

Table 3. The Residual Geolocation Errors Before and After Cal/Val Process for the Two ISSAC Images Shown in Figure 9 with Google Earth™ as the Reference

	Kennedy Space Center, FL			Stanton, ND		
Geolocation	Along-track (m)	Cross-track (m)	Rotational (Deg)	Along-track (m)	Cross-track (m)	Rotational (Deg)
Before cal/val	11461	2660	1.329	14825	3057	1.845
After cal/val	3.85	275.52	0.458	1.53	115.63	0.628

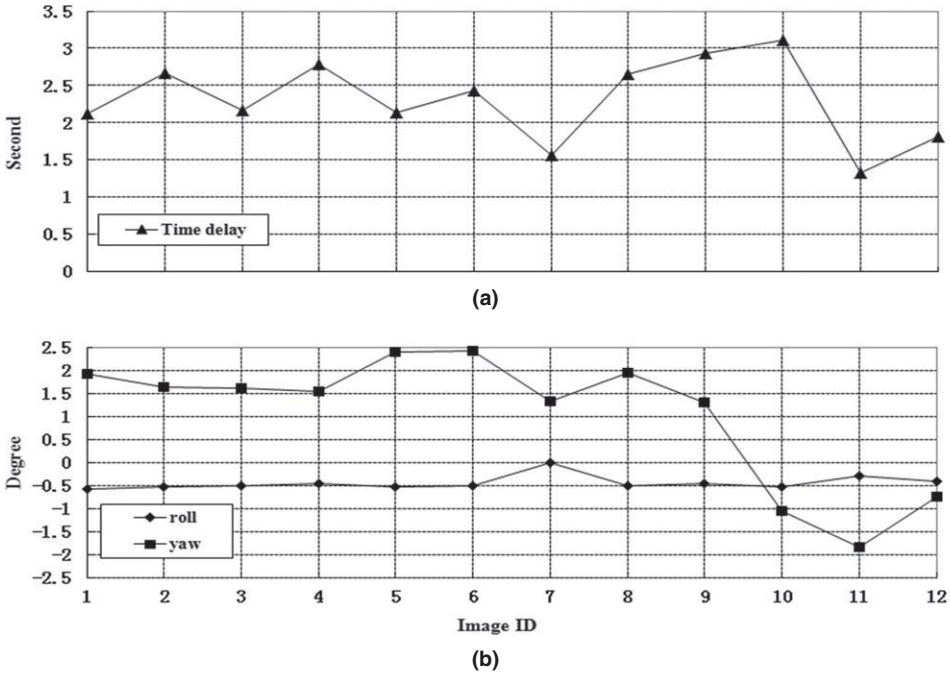

Figure 8. The sources of errors determined by cal/val process that affecting the geolocation accuracy: (a) The temporal offset (seconds) between command issuing and actual image acquisition, and (b) The misalignments of the X-axis (roll, degree) and the Z-axis (yaw, degree) between the ISSAC Sensor CS and the ISS body-fixed CS. A total of 12 images were used with the first nine acquired during ascending orbit and other three descending.

that the ISSAC Sensor CS aligns perfectly with the ISS body-fixed CS in the Y-axis (i.e., pitch = 0). We further assumed that the offset in the cross-track direction (category 2) is due to the misalignment in roll angle and the rotational offset (category 3) due to the misalignment in yaw angle.

Twelve images, acquired over the continental US, were processed using our geolocation algorithm. These images were further processed as described in the following to match the Google Earth™. First, to determine the actual image acquisition time, the recorded "image acquisition" time, which is actually the command issuing time, was increased by 1 millisecond per step. At each interval, the corresponding ISS ephemeral parameters needed by the geolocation algorithm were estimated by linear interpolation and a new location of the ISSAC nadir point was calculated. The temporal offset of image acquisition for the image was determined when the calculated nadir location is the closest to its corresponding reference location on Google Earth™. This would largely eliminate the along-track offset (category 1). Second, the roll angle was adjusted (0.001° per step) to eliminate the residual cross-track difference in the nadir point. Lastly, the yaw angle was adjusted (0.001° per step) to match the four corners of the image. The incremental of 1 millisecond or 0.001° introduces about 6 meters displacement on the ground (roughly the smallest error due to the uncertainty in the ISS orbital state determination).

The results of this preliminary cal/val procedure are shown in Figure 8. The temporal offset in image acquisition varied between approximately one and three seconds. The values are all positive, indicating a delay in actual acquisition of images from the issuing of the acquisition command, as can be expected. The misalignment in the roll angles was relatively consistent among different images, varying slightly around −0.5°. The misalignment in the yaw angle was determined to be about 1.8° and −1.2° for ascending and descending orbits, respectively. As we mentioned earlier, the misalignment between the camera and the ISS should be systematic and independent of the ISS orbit directions. We do not know why the rotational misalignment of images is approximately clockwise for descending cases (e.g., Plate 2a)) and counter-clockwise for the ascending cases (e.g., Plate 2b). The possible reasons could be the ISS drift angle, which measures relative movement of the ISS with respect to the Earth (mainly caused by Earth self-rotation) and has not been considered in the algorithm. Further investigation should be conducted with additional observation, preferably with images obtained in one whole orbit.

The cal/val outcome needs to be applied back to the geolocation algorithm to correct for the uncertainties that we have just quantified. Specifically, values for the roll (r), the pitch (p), and the yaw (y) angles in Equation 4 need to be defined. Based on Figure 8b, we used the mean value of −0.45° for the roll angle, and for the yaw angle the mean value of 1.787° for ascending and −1.217° for descending orbits, respectively. The pitch angle was set to be zero. Since the temporal offset or delay (Figure 8a) is random in nature, its correction has to be applied individually for each image following the procedure described above. These corrections were applied to Plate. 2a and 2c and results are shown Plate 2b and

2d, respectively. As compared in the Table 3, after applying the correction parameters, the geolocation errors in along-track and cross-track directions were reduced from 11.461 and 14.825 km to 3.85 and 1.53 m, and from 2.66 and 3.057 km to 275.52 and 115.63 m, while the rotational offset reduce from 1.329° to 0.458° and from 1.845° to 0.628°, for Kennedy Space Center Florida and Stanton, North Dakota cases, respectively. Among the remaining errors, the largest difference is in the cross-track direction; and the combined error of all three categories is about 500 m after cal/val process, well within the inherent uncertainty of about 800 m due to random errors in determining the ISS ephemeral parameters and the ISSAC off-nadir tilting angles.

Conclusions

A forward geolocation algorithm for the payload onboard the International Space Station (ISS) was developed. Taking advantage of the ISS location and velocity vectors that are directly defined in the CTRS CS, the algorithm transformed the payload look vector from ISS LVLH (orbital) to CTRS (ECR) coordinate system directly, bypassing the intermediate steps of orbital to ECI and ECI to ECR transformation, and thus avoiding the use of the Earth rotation and the ISS ephemeris information, such as polar motion, sidereal time, astronomic nutation, and precession. Furthermore, unit quaternion is used in transforming different coordinate systems, avoiding potential gimbal lock problem potentially associated with the rotation matrix method. The off-nadir tilting angle and pixel coordinate in the CCD array plane of the sensor and the orbital state and attitude information of the ISS are required as input parameters. Comparison with commercial software STK showed that the proposed geolocation algorithm has a theoretical accuracy of within 0.5 m. But the preliminary results as compared with the Google Earth™ indicated an approximate geolocation error of the order of 4 km. The possible sources of the error were analyzed, and we found the largest contribution is due to the misalignment of the ISSAC system with respect to the ISS body-fixed coordinate system. Fortunately, this misalignment error is systematic and fixed once the payload is installed in the ISS. Therefore, these errors can be modeled and corrected for through ground-based cal/val process. The other possible error sources are random in nature and include the inherent uncertainties in ISS attitude and position determinations, ISSAC tilting angle, and image acquisition time. The uncertainties in ISS orbit status would cause a geolocation error on the order of 700 m, and those in ISSAC tilting angle would cause an error of 70 m at most.

The preliminary val/cal process using Google Earth™ as reference indicated that there is always a delay of 1 to 3 seconds in the execution of image acquisition command, which results in a about 20 km shift of images in along-track directions. This is largely because that the Windows® operating environment, in which the ISSAC control software was developed, is not a real-time system. Therefore, the actual command execution always lags behind the command issuing, even though the amount of delay varies. Upon the time delay being compensated, the misalignment in the X-axis (roll) and Z-axis (yaw) of ISSAC Sensor CS with respect to the ISS body-fixed CS were determined to be 0.45° and 1.787°/ascending or –1.217°/descending. After correcting for these errors, the geolocation accuracy can be achieved of approximately 500 meters. The algorithm was originally developed for the ISSAC sensor, but it can be applied to other Earth observing sensors onboard ISS with no or minor changes.

Acknowledgments

This work was supported in part by the National Basic Research "973" program of China under contract 2009CB723903 and the National Natural Science Foundation of China under contract 61132006. The ISSAC project was funded by the National Aeronautics and Space Administration through Grant NNX10AH20G and related prior grants. We would like to acknowledge the extensive contributions of the students and faculty of the University of North Dakota who contributed to the design, development, and operation of ISSAC. We also would like to thank staff from NASA for their cooperation and helping in ISSAC project, and Dr. Chunming Han and Haitao Zhao from CEODE, CAS for the valuable discussion. The study was mainly carried out while Changyong Dou was a visiting scholar at the University of North Dakota.

References

Corson, M.R., R.L. Lucke, C.O. Davis, J.H. Bowles, D.T. Chen, B. Gao, D.R. Korwan, W.D. Miller, and W.A. Snyder, 2010. The Hyperspectral Imager for the Coastal Ocean (HICO™) environmental littoral imaging from the International Space Station, *Proceedings of IGARSS'10*, 25-30 July, Hawaii.

Gebelein, J., and D. Eppler, 2006. How Earth remote sensing from the International Space Station complements current satellite-based sensors, *International Journal of Remote Sensing*, 27(13): 2613–2629.

Hanson, A.J., 2000. *Visualizing Quaternions*, Morgan Kaufmann, Elsevier Inc., San Francisco, 55 p.

Hart, J.C., G.K. Francis, and L.H. Kauffman, 1994. Visualizing quaternion Rotation, *ACM Transactions on Graphics*, 13(3):256–276.

Jacobson, C.A., 2007. International Space Station remote sensing pointing analysis, *Proceedings of the IEEE Aerospace Conference'07*, 03-10 March, Big Sky, Montana.

Jules, K., 2008. Summary of the science performed onboard the International Space Station during increments 12 and 13, *Acta Astronautica*, 63:38–52.

Kieffer, H.H., K.F. Mullins, and D.J. Mackinnon, 2008. Validation of the ASTER instrument level 1A scene geometry, *Photogrammetric Engineering & Remote Sensing*, 74(3):289–301

Lee, C., H.J. Theiss, J.S. Bethel, and E.M. Mikhail, 2000. Rigorous mathematical modeling of airborne pushbroom imaging systems, *Photogrammetric Engineering & Remote Sensing*, 74(3):303–309

Olsen, D., C. Dou, X. Zhang, L. Hu, H. Kim, and E. Hildum, 2010. Radiometric calibration for AgCam, *Remote Sensing*, 2(2):464–477.

Olsen, D.R., H.J. Kim, J. Ranganathan, and S. Laguette, 2011. Development of a low-cost student-built multi-spectral sensor for the International Space Station, *Proceedings of SPIE 8153, 815300,* 23 August, San Diego, California.

Poe, G.A., E.A. Uliana, B.A. Gardiner, T.E. VonRentzell, and D.B. Kunkee, 2008. Geolocation error analysis of the special sensor microwave imager/sensor, *IEEE Transactions on Geoscience and Remote Sensing*, 46(4):913–922.

Polites, M.E., and B.E. Bartlow, 1997. *United States Control Module Guidance, Navigation, and Control Subsystem Design Concept*, National Aeronautics and Space Administration, Marshall Space Flight Center, Alabama.

Potere, D., 2008. Horizontal positional accuracy of Google Earth's high-resolution imagery Archive, *Sensors*, 8(12):7973–7981.

Reibaldi, G.G., G. Gianfiglio, S. Feltham, and P.C. Galeone, 2004. The ESA pressurized and unpressurized payloads in the Columbus laboratory, *Proceedings of the 55*th International Astronautical Congress, 04-08 October, Vancouver, Canada.

Robinson, J.A., D.L. Amsbury, D.A. Liddle, and C.A. Evans, 2002. Astronaut-acquired orbital photographs as digital data for remote sensing: Spatial resolution, *International Journal of Remote Sensing*, 23(20):4403–4438.

Robinson, J.A., B. McRay, and K.P. Lulla, 2000. Twenty-eight years of urban growth in North America quantified by analysis of photographs from Apollo, Skylab and Shuttle-Mir, *Dynamic Earth Environments: Remote Sensing Observations from Shuttle-Mir Missions* (K.P. Lulla and L.V. Dessinov, editors.), John Wiley & Sons Inc., New York, pp. 25–41, 262, 269–270.

Rosborough, G.W., D.G. Baldwin, and W.J. Emery, 1994. Precise AVHRR image navigation, *IEEE Transactions on Geoscience and Remote Sensing*, 32(3):644–657.

Sauceda, F., G.B. Ray, B. Korin, N. Wilks, and L. Delheimer, 2001. International Space Station Program (SSP 30219) - Space Station Reference Coordinate Systems, URL: *http://www.asi.org/adb/04/02/00/iss-coordinate-systems.pdf* (last date accessed: 09 April 2013).

Stefanov, W.L., J.A. Robinson, and S.A. Spraggins, 2003. Vegetation measurements from digital astronaut photography, *Proceedings of the International Archives of the Photogrammetry, Remote Sensing, and Spatial Information Sciences*, 34 (7/W9):185–189.

Tank, V., D. Oertel, B. Zhukov, F. Shreier, K. Beier, P. Haschberger, E. Lorenz, W. Skrbek, and H. Jahn, 2001. FOCUS on ISS-sensor and data fusion for Earth observation from space, *Proceedings of IEEE International Conference on Multisensor Fusion and Integration for Intelligent Systems*, 01 August, Germany.

Vajdos, G., M. Begley, D. Cupitt, and R. Loffi, 2004. *ISS Guidance, Navigation, and Control System White Paper Navigation Data Accuracy and Characteristics for Payload Support*, National Aeronautics and Space Administration.

Wiebe, H., G. Heygster, and L. Meyer-Lerbs, 2002. Geolocation of AMSR-E data, *IEEE Transactions on Geoscience and Remote Sensing*, 46(10):3098–3103.

Wolfe, R.E., M. Nishama, A.J. Fleig, J.A. Kuyper, D.P. Roy, J.C. Storey, and F.S. Patt, 2002. Achieving sub-pixel geolocation accuracy in support of MODIS land science, *Remote Sensing of Environment*, 83:31–49.

Zhang, X., S. Seelan, and G. Seielstad, 2010. Digital northern great plains: A web-based system delivering near real time remote sensing data for precision agriculture, *Remote Sensing*, 2(3), 861–873.

(Received 24 February 2012; accepted 18 January 2013; final version 31 January 2013)

ASPRS Code of Ethics

Honesty, justice, and courtesy form a moral philosophy which, associated with mutual interest among people, should be the principles on which ethics are founded.

Each person who is engaged in the use, development, and improvement of the mapping sciences (Photogrammetry, Remote Sensing, Geographic Information Systems, and related disciplines) should accept those principles as a set of dynamic guides for conduct and a way of life rather than merely for passive observance. It is an inherent obligation to apply oneself to one's profession with all diligence and in so doing to be guided by this Code of Ethics.

Accordingly, each person in the mapping sciences profession shall have full regard for achieving excellence in the practice of the profession and the essentiality of maintaining the highest standards of ethical conduct in responsibilities and work for an employer, all clients, colleagues and associates, and society at large, and shall . . .

1. Be guided in all professional activities by the highest standards and be a faithful trustee or agent in all matters for each client or employer.
2. At all times function in such a manner as will bring credit and dignity to the mapping sciences profession.
3. Not compete unfairly with anyone who is engaged in the mapping sciences profession by:
   a. Advertising in a self-laudatory manner;
   b. Monetarily exploiting one's own or another's employment position;
   c. Publicly criticizing other persons working in or having an interest in the mapping sciences;
   d. Exercising undue influence or pressure, or soliciting favors through offering monetary inducements.
4. Work to strengthen the profession of mapping sciences by:
   a. Personal effort directed toward improving personal skills and knowledge;
   b. Interchange of information and experience with other persons interested in and using a mapping science, with other professions, and with students and the public;
   c. Seeking to provide opportunities for professional development and advancement of persons working under his or her supervision;
   d. Promoting the principle of appropriate compensation for work done by person in their employ.
5. Undertake only such assignments in the use of mapping sciences for which one is qualified by education, training, and experience, and employ or advise the employment of experts and specialists when and whenever clients' or employers' interests will be best served thereby.
6. Give appropriate credit to other persons and/or firms for their professional contributions.
7. Recognize the proprietary, privacy, legal, and ethical interests and rights of others. This not only refers to the adoption of these principles in the general conduct of business and professional activities, but also as they relate specifically to the appropriate and honest application of photogramme try, remote sensing, geographic information systems, and related spatial technologies. Subscribers to this code shall not condone, promote, advocate, or tolerate any organization's or individual's use of these technologies in a manner that knowingly contributes to:
   a. deception through data alteration;
   b. circumvention of the law;
   c. transgression of reasonable and legitimate expectation of privacy.